Modeling of the heat transfer of a Solar Multi-effect Distillation Plant at the Plataforma Solar de Almería

Patricia Palenzuela, Diego Alarcón, Julián Blanco, Elena Guillén, Mercedes Ibarra, Guillermo Zaragoza*.

CIEMAT-Plataforma Solar de Almería, Ctra. de Senés s/n, 04200 Tabernas, Almería, Spain.

*Corresponding author. Tel.: +34 950387941; fax: +34 950365015. *Email address*: guillermo.zaragoza@psa.es

Email addresses: patricia.palenzuela@psa.es, diego.alarcon@psa.es, julian.blanco@psa.es, guillermo.zaragoza@psa.es, elena.guillen@psa.es, mercedes.ibarra@psa.es

Abstract

Potable water supply by desalination systems has a significant role in today's developing world. Multi-effect distillation (MED) is a progressing, low cost and easy operating system to produce drinking and pure water for both social and industrial applications. It is very important to understand in detail the process elements in order to determine the effects of the important design and operating variables on the parameters controlling the performance of the plant. A model is developed for the MED plant located at the Plataforma Solar de Almería (PSA), in the southeast of Spain. It is a vertical-arrangement forward-feed MED plant with pre-heaters, which uses hot water as the thermal energy source. The model has been developed dividing the MED plant into four blocks: the heater (consisting of the first effect), the evaporators (consisting of effects 2 to N), the pre-heaters (for effects 1 to N-1) and the condenser (after effect N). To solve the model, a parameterization of the overall heat transfer coefficient of the four blocks has been carried out with experimental data for a wide range of operation, based on correlations found by other authors for similar plants. The adjustments were good for all the components with the exception of the condenser, which seems to behave differently than in other cases reported in the literature.

Keywords: Solar desalination; Multi-effect distillation; Modeling

1. Introduction

The desalination industry plays a fundamental role in the struggle against the high water stress that many areas of the world are experiencing. It appears as a solution for providing a reliable source of fresh water in places with seawater availability. Thermal desalination processes have been used commercially for more than half a century now. They are intensive energy consumers, so an effective incorporation of renewable energies is required to guarantee the sustainability of this technological option. The usual coincidence in many locations of fresh water shortage, abundant seawater resources and high isolation levels makes thermal seawater desalination driven by solar energy one of the most promising processes to obtain fresh water. This can be possible by the coupling of a conventional thermal desalination technology with a solar thermal system [1]. Within these processes, multi-effect distillation (MED) has acquired a stronger interest over multi-stage flash (MSF), since the former is more efficient from a thermodynamic and heat-transfer point of view. The pumping power and the specific heat transfer area required for the MED system are about 20% and 50% of that needed for the MSF system [2, 3]. Moreover, MED plants have the same performance ratio than MSF plants, needing the former less effects than the latter. Therefore, the capital cost of the MED system is expected to be lower than that of MSF systems.

To get the largest efficiency from the MED process, it is necessary to understand in detail the process elements in order to improve future designs and to predict the performance over a wide range of possible operating conditions. Mathematical modeling and computer simulations can provide an insight into the workings of the system. Some authors have published the modeling and simulation of a MED system. A steady-state analysis for the process was carried out assuming constant transfer areas for evaporators and pre-heaters in all effects, variation in thermodynamic losses from one effect to another, dependence of the physical properties of water on salinity and temperature, and influence of non-condensable gases on the heat transfer coefficients in the evaporators and the feed pre-heaters [4]. A mathematical simulation of the steady-state operation of a MED plant was presented [5], which was validated with experimental data from a plant located at Abu Dhabi, UAE. The agreement between the

theory and the test results was found to be satisfactory. Also, a steady state mathematical model of a multi-effect distillation with thermal vapor compression (MED-TVC) was developed to evaluate the model system performance [6]. The model validity was examined against three commercial MED-TVC plants, showing acceptable results.

This paper presents the work done on a model of the MED plant located at the Plataforma Solar de Almería (PSA), in the southeast of Spain. To solve the model, a parameterization of the overall heat transfer coefficient of the heater, the evaporators, the pre-heaters and the end condenser has been carried out with experimental data for a wide range of operation.

2. Description of the plant

2.1 Process design

The desalination plant of PSA is a forward-feed MED unit manufactured and delivered by ENTROPIE in 1987 [7]. It has 14 cells, or effects, in a vertical arrangement at decreasing pressures from cell 1 to cell 14 [8]. The original first effect worked with low-pressure saturated steam (70ºC, 0.31 bars). In 2005 it was replaced by a new one, which is able to work with hot water as heat transfer media [9]. The required heat for the first cell is provided either with a solar field composed of static compound parabolic concentrators (CPC) or with a double effect absorption heat pump, DEAPH (LiBr-H2O) which was manufactured by ENTROPIE in 2005 in the framework of the AQUASOL project [10, 11, 12]
The flow sheet of the process is shown in Fig 1. Feed seawater is preheated and pumped to the first cell where seawater is flown through a spraying tray over a horizontal-tube bundle, building a thin falling film which coats the surface of the tubes entirely. Then, evaporation of part of the seawater is driven by the release of the sensible heat of the hot water. Vapor generated in the first effect flows to the pre-heater located next to it, through a wire mesh demister which removes the entrained brine droplets. Here, vapor transfers part of its latent heat to the seawater which is circulating inside the pre-heater tube bundle, increasing its temperature. As a consequence, a small amount of the vapor condenses, and the vapor which has not condensed flows through the inside of the second effect tube bundle, where it condenses by transferring its latent heat to the more concentrated brine flowing from the previous effect and being sprayed on the outside surface of the tube bundle.

The heat transfer in the rest of effects is made by the vapor produced in the previous effect. The vapor generated in the last effect is led to the end condenser, where is condensed by transferring the latent heat of evaporation to the cooling seawater which is passing through the condenser tube bundle. That heated seawater is divided into two streams, some is pumped to the first effect of the plant after passing through the pre-heaters of each effect and the rest is rejected.

All the condensation (distillate) obtained in each effect goes to the next one with the following exceptions: in the fourth cell the distillate is extracted to recover its sensible heat, part of it goes to the seventh cell and the rest to the tenth. Similar extraction is made in the seventh cell, splitting the condensate between the tenth and the thirteenth effects. Another extraction takes place from the tenth cell, part goes to the thirteenth effect and the rest is mixed with the distillate produced in the fourteenth effect. The final extraction is made in the thirteenth effect, after which all the distillate is mixed with that produced in the fourteenth effect.

Besides the vapor formed by boiling, a small portion is formed by flashing. When the brine pass from one effect to another, some flashing takes place since it enters a cell which is at a lower pressure than the previous one.

In order to remove the non-condensable gases, a hydro-ejectors vacuum-producing system is installed, connected to effects 2, 7 and the end condenser. This system establishes the vacuum required for operation.

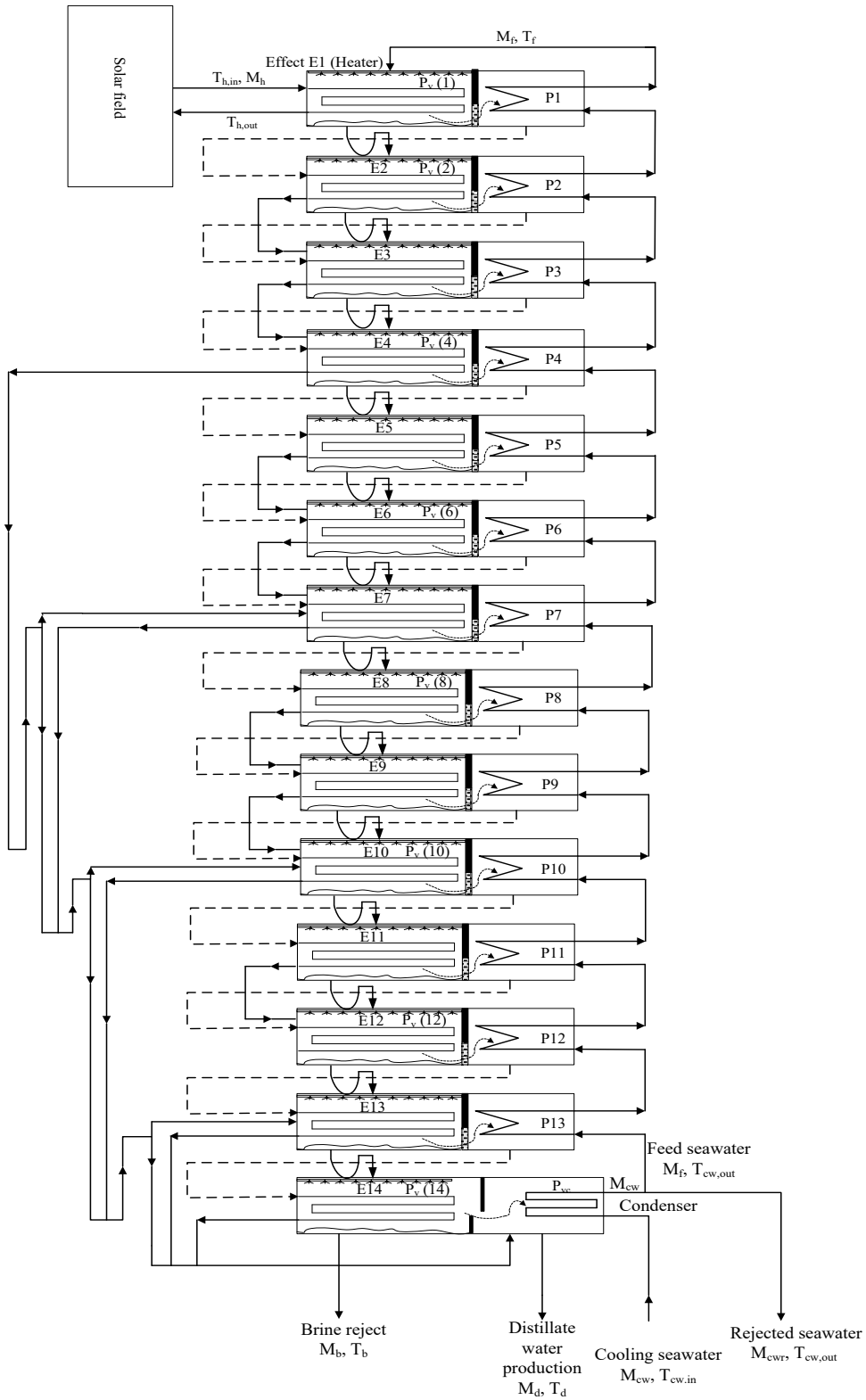

Fig 1. Schematic diagram of the multi-effect distillation plant at the Plataforma Solar de Almería. Dashed lines show the steam flow; solid lines the distillate flow; U-shaped lines represent the brine flow from one effect to the next.

The design specifications of the PSA MED plant are given in Table 1. The tube bundles of the heater, evaporators, pre-heater and condenser are made of 90-10 Cu-Ni tubes. The surface areas of each of the different tube bundles are:

- Heater evaporator bundle, 24.26 m^2.

- Effect 2-14 evaporator bundle, 26.28 m^2.
- Pre-heater bundle, 5 m^2.
- Condenser bundle, 18.3 m^2.

Table 1
Design specifications of the MED-PSA plant.

Number of effects	14
Feed seawater flow rate	8 m^3/h
Brine flow rate from the last effect	5 m^3/h
Hot water flow rate	12.0 L/s
Total distillate output	3 m^3/h
Cooling seawater flow rate at 25 ºC	20 m^3/h
Vapor production in the last effect at 70 ºC	159 kg/h
Heat source energy consumption	200 kW
Performance ratio	> 9
Vacuum system	Hydro-ejectors (seawater at 3 bar)
Inlet/Outlet hot water temperature	74.0/70.0 ºC
Brine temperature (on the first cell)	68 ºC
Feed and cooling seawater temperature at the outlet of the condenser	33 ºC

2.2 Experimental set-up

The MED-PSA plant is experimental and therefore equipped with a comprehensive monitoring system, which provides instantaneous values of the measured data. The monitored data are detailed in Table 2 and are also indicated in Fig 1. The supply water to the desalination plant is obtained from wells and stored in a pool from where the cooling water is pumped to the tube bundle of the condenser. Afterwards, part of it is used as feed water in the first effect and the rest is rejected back to the pool. Therefore, part of the heat released at the condenser goes into the pool and the cooling water temperature could increase during the experiment, which is not desirable. To avoid that, a dry cooler is switched on since the beginning of the experiment cooling the pool.

Table 2
Monitored data at PSA MED plant

Measurement	Name of variable	Magnitude
Flow rate:	M_h	Heating water flow
	M_{cw}	Cooling seawater flow
	M_{cwr}	Rejected seawater flow
	M_f	Feed seawater flow
	M_d	Product water flow
	M_b	Brine flow
Temperature:	$T_{h,in}$	Heating water inlet
	$T_{h,out}$	Heating water outlet
	T_f	1st effect sprayed seawater temp.
	$T_{cw,in}$	Cooling seawater inlet temp.
	$T_{cw,out}$	Cooling seawater (rejected) outlet temp.
Pressure:	$P_v(1)$, $P_v(2)$, $P_v(4)$, $P_v(6)$, $P_v(8)$, $P_v(10)$, $P_v(12)$, $P_v(14)$	1st, 2th, 4th, 6th, 8th, 10th, 12th, 14th effect vapor press.
	P_{vc}	Vapor pressure in the condenser
Salt concentration:	X_f	Seawater TDS at the condenser inlet

As the model proposed is at steady-state, time averages of the measured data are carried out in order to perform the modeling.

3. Mathematical model

The model has been implemented in MATLAB environment accounting for the processes and features of the MED-PSA plant. The following assumptions have been taken into account in order to simplify the analysis: steady state operation, negligible heat losses to the surroundings, equal temperature difference across the effects, equal temperature difference across the pre-heaters, salt-free distillate from all the effects and negligible boiling point elevation and non-equilibrium allowance due to the low salt concentration of the supply water in this plant. Steady state mass and energy balances have been set out for all the components of the plant, based on the work developed by [13], though the first effect has been modeled taking into account that this unit uses hot water as the thermal energy source. To develop the model, the MED system has been divided into four blocks: the heater (consisting of the first effect), the evaporators (consisting of effects 2 to N), the pre-heaters (for effects 1 to N-1) and the end condenser (after effect N). The overall brine, salt and energy balances for each of these blocks are given below.

3.1 The heater

Fig 2 shows a schematic diagram of the heater, which corresponds to the first effect of the plant.

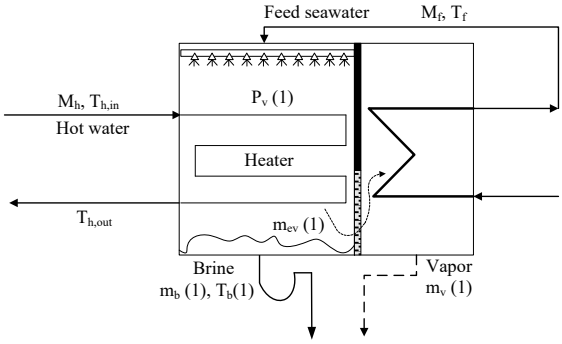

Fig 2. Flow diagram of the heater (effect 1)

The overall mass balance to determine the brine flow rate leaving the first effect ($m_b(1)$) can be written as follows:

$$m_b(1) = M_f - m_{ev}(1) \tag{1}$$

where M_f is the feed seawater flow rate and $m_{ev}(1)$ the vapor mass flow rate which leaves the heater.

The salt mass conservation law is applied, therefore assuming that the distillate is free of salt, the salinity of the brine leaving the heater ($X(1)$) is:

$$X(1) = \frac{X_f M_f}{m_b(1)} \tag{2}$$

where X_f is the feed seawater salinity.

The energy balance of the heater is given by:

$$Q_h = M_h \cdot (h_{in} - h_{out}) = m_b(1) \cdot h_b(1) - M_f \cdot h_f + m_{ev}(1) \cdot \lambda_v(1) \tag{3}$$

where M_h is the hot water mass flow rate from the CPC solar field.

The temperature of the vapor generated in the heater, $T_v(1)$, is lower than that of the non-evaporated brine, $T_b(1)$, by the boiling point elevation (BPE). Therefore:

$$T_b(1) = T_v(1) + BPE \tag{4}$$

The heat transfer equation for the heater can be written as:

$$Q_h = A_h \cdot U_h \cdot \frac{T_{h,in} - T_{h,out}}{\ln\left(\frac{T_{h,in} - T_v(1)}{T_{h,out} - T_v(1)}\right)} \tag{5}$$

where U_h is the overall heat transfer coefficient for the heater.

3.2 The pre-heaters

Fig 3 shows the flow diagram of a typical pre-heater.

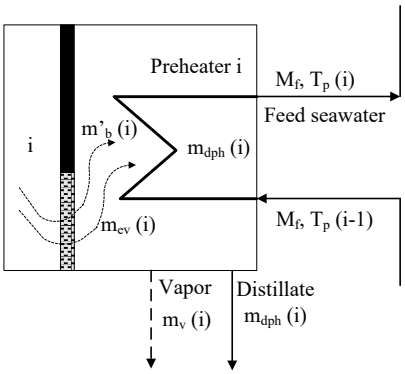

Fig 3: Flow diagram of a typical pre-heater

The temperature difference between pre-heaters is assumed to be the same for all of them and can be calculated as follows:

$$\Delta T_p = \frac{T_f - T_{cw,out}}{N-1} \tag{6}$$

where $T_{cw,out}$ is the outlet cooling seawater temperature from the condenser, which is equal to the inlet seawater temperature to the last pre-heater ($T_p(N-1)$), T_f is the outlet seawater temperature from the first pre-heater ($T_p(1)$). Then, the seawater temperature in each pre-heater can be calculated as follows:

$$T_p(i) = T_p(i-1) + \Delta T_p \tag{7}$$

The energy conservation equation for a typical pre-heater (i=1,N-2) is given below:

$$Q_p(i) = M_f \cdot (h_p(i) - h_p(i-1)) = m_{dph}(i)\lambda_{ph}(i) \tag{8}$$

where $m_{dph}(i)$ is the amount of distillate that is produced in the pre-heater due to the transfer of energy from the vapor to the feed seawater which is flowing through the bundle tube of the pre-heater.

In the case of the last pre-heater (i=N-1) the inlet temperature is the outlet temperature of the condenser, so the energy balance can be written as:

$$Q_p(N-1) = M_f \cdot (h_p(N-1) - h_{cw,out}) = m_{dph}(i)\lambda_{ph}(i) \tag{9}$$

The overall mass balance to determine the vapor mass flow rate leaving the pre-heater ($m_v(i)$) can be written as follows:

$$m_v(i) = m_{ev}(i) + m_b^{'}(i) - m_{dph}(i) \tag{10}$$

where $m^{'}_b$ is the amount of vapor formed by flashing of the brine passing from one effect to the other. In the case of the vapor leaving the first pre-heater the second term of this equation is zero, as no vapor is formed by flash of the seawater that enters the heater.

The heat transfer equation for a typical pre-heater (i=1,N-1) is written as follows:

$$Q_p(i) = A_p \cdot U_p(i) \frac{\left(T_v(i) - T_p(i-1)\right) - \left(T_v(i) - T_p(i)\right)}{\ln\left(\frac{T_v(i) - T_p(i-1)}{T_v(i) - T_p(i)}\right)} \tag{11}$$

where $U_p(i)$ is the overall heat transfer coefficient for a typical pre-heater.

3.3 The evaporators

The temperature difference across the effects is assumed to be the same in all of them and can be calculated as follows:

$$\Delta T_v = \frac{T_v(1) - T_v(N)}{N-1} \tag{12}$$

Then, the vapor temperature in each evaporator (i=1,N) can be calculated as follows:

$$T_v(i) = T_v(i-1) - \Delta T_v \tag{13}$$

As in equation (4), the brine temperature is given by:

$$T_b(i) = T_v(i) + BPE \tag{14}$$

The amount of distillate that leaves each effect is different depending on the number of effect:

For those effects in which distillate from the previous effect enters in (effects 3rd, 4th, 6th, 9th and 12th), the amount of distillate is given by:

$$m_d(i) = m_v(i-1) + m_{dph}(i-1) + m_d(i-1) \tag{15}$$

In the case of the effects in which no distillate from the previous effect enters (2nd, 5th, 8th, 11th and 14th), the amount of distillate is:

$$m_d(i) = m_v(i-1) + m_{dph}(i-1) \tag{16}$$

As it was mentioned in section 2, in cells 7th, 10th and 13th, outlet and inlet of distillate take place, which can be seen in detail in Fig. 4.

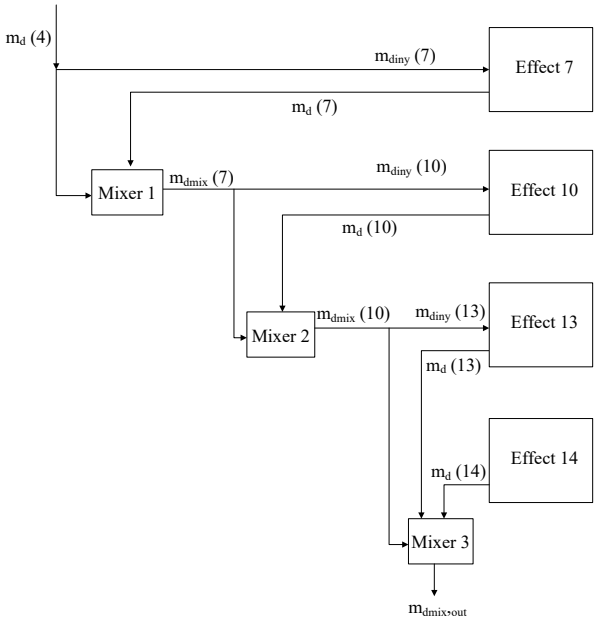

Fig 4: Flow diagram of the extractions

For these effects, the amount of distillate that leaves each effect is given by:

$$m_d(i) = m_v(i-1) + m_{dph}(i-1) + m_d(i-1) + m_{diny}(i) \tag{17}$$

The distillate mass flow rate that enters in cells 7th, 10th and 13th ($m_{diny(i)}$) can be determined by mass balances in the mixers:

Effect 7:

$$m_{diny}(7) = y \cdot m_d(4) \tag{18}$$

$$m_{dmix}(7) = (1-y) \cdot m_d(4) + m_d(7) \tag{19}$$

Effect 10:

$$m_{diny}(10) = y \cdot m_{dmix}(7) \tag{20}$$

$$m_{dmix}(10) = (1-y) \cdot m_{dmix}(7) + m_d(10) \tag{21}$$

Effect 13:

$$m_{diny}(13) = y \cdot m_{dmix}(10) \tag{22}$$

Finally, the mass balance in the last mixer is as follows:

$$m_{dmix,out} = (1-y) \cdot m_{dmix}(10) + m_d(13) + m_d(14) \tag{23}$$

In all the equations above, y is the percentage of distillate which enters in the effect. It is considered to be 1.5%. Regarding the brine, for effects 2 to N, the brine flow rate leaving effect i is given by:

$$m_b(i) = M_f - \sum_{i=1}^{N} m_{ev}(i) - \sum_{i=2}^{N} m'_b(i) \tag{24}$$

The mass flow rate of vapor formed by brine flashing in the flash box is given by:

$$m'_b(i) = m_b(i-1) \cdot \frac{h_{liqsat}(T_b(i-1)) - h_{liqsat}(T'_b(i))}{\lambda'_b(i)} \tag{25}$$

where T'_b is the temperature of flashing brine which is higher than the boiling temperature within the effect, T_b, by the non-equilibrium allowance, which is a measure of the flashing process [4]:

$$T'_b(i) = T_b(i) + NEA \tag{26}$$

In equation(25), λ'_b is the latent heat of formed vapor at T'_b.

The salt balance in the brine stream leaving effects 2 to N is:

$$X(i) = \frac{M_f X_f}{M_f - \sum_{i=1}^{N} m_{ev}(i) - \sum_{i=2}^{N} m'_b(i)} \tag{27}$$

The energy balances in the evaporators can be written as follows:
For those effects in which distillate from the previous effect enter in (effects 3rd, 4th, 6th, 9th and 12th) (see Fig 5):

$$Q_{ev}(i) = m_{ev}(i)\lambda_v(i) = \left(m_v(i-1)\cdot\lambda_v(i-1)\right) + m_{br}(i-1)\cdot h_{liqsat}(T_v(i)) - m_b(i)\cdot h_{liqsat}(T_b(i)) + \tag{28}$$
$$m_{dph}(i-1)\cdot(h_{liqsat}(T_v(i-1)) - h_{liqsat}(T_v(i))) + m_d(i-1)\cdot(h_{liqsat}(T_v(i-1)) - h_{liqsat}(T_v(i)))$$

where $m_{ev}(i)$ is the amount of vapor produced by boiling; $m_{br}(i)$ is the brine mass flow rate that has not flashed in the flash box, so it is sprayed over the evaporator.

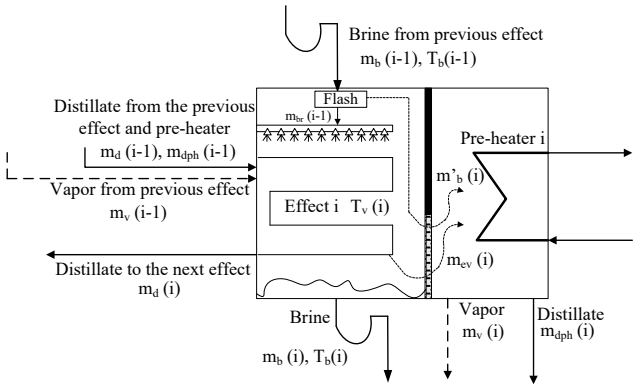

Fig 5. Flow diagram of the evaporators 3rd, 4th, 6th, 9th and 12th

In the case of the effects in which no distillate from the previous effect enters (2nd, 5th, 8th, 11th and 14th), the energy balance is (see Fig 6):

$$Q_{ev}(i) = m_{ev}(i)\lambda_v(i) = \left(m_v(i-1)\cdot\lambda_v(i-1)\right) + m_{br}(i-1)\cdot h_{liqsat}(T_v(i)) - m_b(i)\cdot h_{liqsat}(T_b(i)) + m_{dph}(i-1)\cdot(h_{liqsat}(T_v(i-1)) - h_{liqsat}(T_v(i))) \quad (29)$$

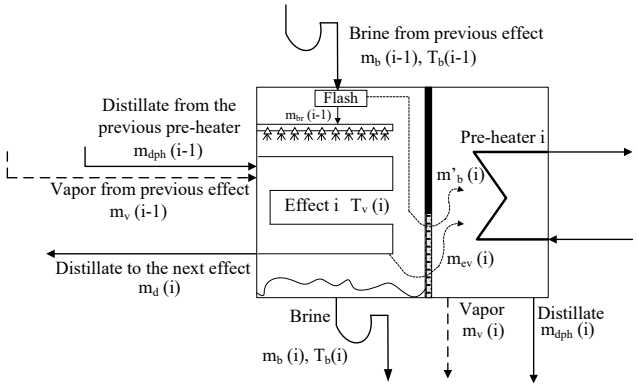

Fig 6. Flow diagram of the evaporators 2nd, 5th, 8th, 11th and 14th

Finally, in those effects in which additional distillate from other effects enters (7th, 10th, 13th), an additional amount of distillate, $m_{diny(i)}$, has to be taken into account (see Fig 7):

$$Q_{ev}(i) = m_{ev}(i)\lambda_v(i) = \left(m_v(i-1)\cdot\lambda_v(i-1)\right) + m_{br}(i-1)\cdot h_{liqsat}(T_v(i)) - m_b(i)\cdot h_{liqsat}(T_b(i)) + m_{dph}(i-1)\cdot(h_{liqsat}(T_v(i-1)) - h_{liqsat}(T_v(i))) + m_{diny}(i)\cdot(h_{liqsat}(T_v(i-3)) - h_{liqsat}(T_v(i)) \quad (30)$$

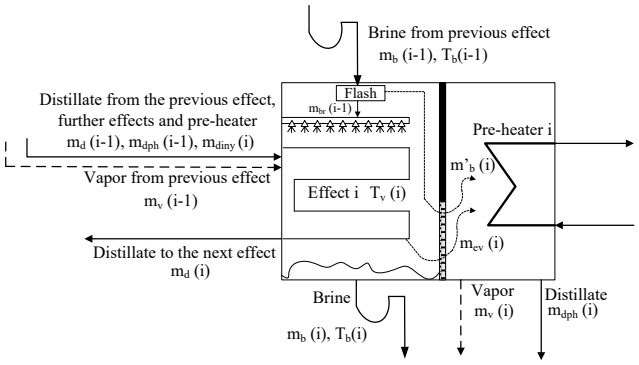

Fig 7. Flow diagram of the evaporators 7th, 10th and 13th

The heat transfer equation for a typical evaporator E_i can be expressed as:

$$Q_{ev}(i) = U_{ev}(i)A_{ev}(i)\cdot(T_v(i-1) - T_v(i) + BPE) \quad (31)$$

where $U_{ev}(i)$ is the overall heat transfer coefficient of a typical evaporator.

3.4 The end condenser

The energy conservation equation for the condenser (Fig 8) is given below:

$$Q_c = M_{cw}\cdot(h_{cw,out} - h_{cw,in}) = m_{dcond}\cdot\lambda_v \quad (32)$$

where m_{dcond} is the total vapor that leaves the 14th evaporator and condenses in the end condenser:

$$m_{dcond} = m_{ev}(N) + m_b^{'}(N) \quad (33)$$

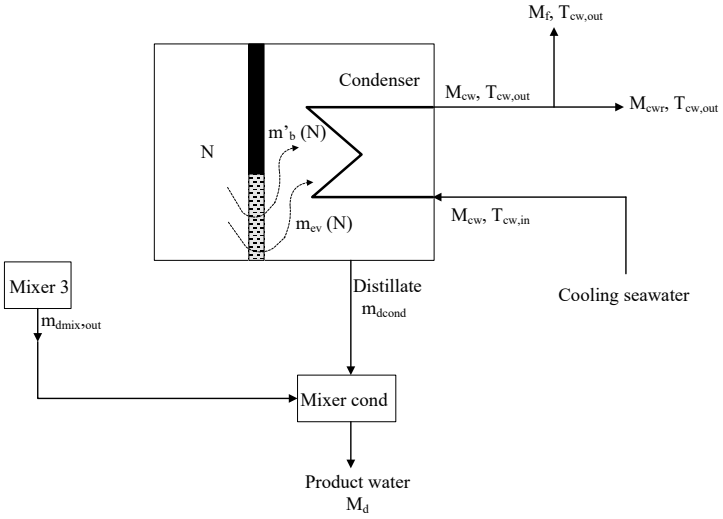

Fig 8: Flow diagram of the end condenser

The total distillate output is:

$$M_d = \sum m_d(i) + m_{dmix,out} + m_{dcond} \tag{34}$$

where the distillate mass flow rate from each effect ($m_d(i)$) is calculated by the equations 15-22.

The heat transfer equation of the condenser is:

$$Q_c = A_c \cdot U_c \frac{\left(T_v(N) - T_{cw,in}\right) - \left(T_v(N) - T_{cw,out}\right)}{\ln\left(\frac{T_v(N) - T_{cw,in}}{T_v(N) - T_{cw,out}}\right)} \tag{35}$$

where U_c is the overall heat transfer coefficient of the condenser.

The overall mass balance equations are given as follows:

$$M_f = m_b(N) + M_d \tag{36}$$

$$X_b = \frac{X_f M_f}{m_b(N)} \tag{37}$$

The performance ratio of the plant is defined as the kilograms of distillate produced for every 2326 kJ of thermal energy supplied to the system. Therefore, the equation to assess it is:

$$PR = \frac{M_d}{Q_h} \times \frac{2326kJ}{1kg} \tag{38}$$

4. Parameterization

To run the model described above, the overall heat transfer coefficients of the first effect (heater), of all pre-heaters 1 through 13, of evaporators bundles in effects 2 through 14 and of the condenser are needed (equations (5), (11), (31) and (35)). Therefore, a parameterization of the coefficients with the input parameters of the model has been made by performing several experiments at the MED-PSA plant.

The experiments have been carried out for different values of the heating water temperature ($T_{h,in}$ in a range of 57ºC-75ºC), the cooling seawater temperature ($T_{cw,in}$ between 12ºC and 25ºC), the heating water flow rate (M_h in a range between 7.8 L/s and 12 L/s), the feed water flow rate (M_f between 6 m^3/h and 8 m^3/h), and the cooling seawater flow rate (M_{cw} between 10 m^3/h and 25 m^3/h).

The correlations of the overall heat transfer coefficients are based on the characterization published by El-Nashar (2000). Therefore, for the first effect the overall heat transfer coefficient U_h (kW/m^2ºC) was adjusted as a function of the feed seawater flow rate, M_f (kg/s), the heating water flow rate, M_h (kg/s), and the inlet heating water temperature, $T_{h,in}$ (ºC). For the condenser, the overall heat transfer coefficient U_c (kW/m^2ºC) was analyzed in terms of the average seawater temperature in the condenser (($T_{cw,in}$+$T_{cw,out}$)/2)).

For the pre-heaters an average overall heat transfer coefficient U_p (kW/m^2ºC) can be calculated by considering the global heat transfer in all 13 pre-heaters (Q_p):

$$U_p = \frac{Q_p}{A_p \times \Delta T_p \times (N-1)} \tag{39}$$

Where A_p is the tube surface area of each pre-heater, ΔT_p is the temperature difference of each pre-heater, which is assumed to be the same in all of them (equation (6)), and Q_p is the heat transfer rate in the 13 pre-heaters, which is calculated by:

$$Q_p = M_f \cdot (h_f - h_{cw,out}) \tag{40}$$

The overall heat transfer coefficient of the pre-heaters, U_p was correlated with the feed seawater flow, M_f (kg/s) and a pre-heater average water temperature $\overline{T}_p$ (mean between the seawater at the inlet of the last pre-heater, $T_{cw,out}$, and at the outlet of the first one, T_f).

Similarly, for the evaporators (effects 2 through 14) an average overall heat transfer coefficient, U_{ev} (kW/m^2ºC), can be calculated by considering the global heat transfer in all 13 evaporators (Q_{ev}):

$$U_{ev} = \frac{Q_{ev}}{A_{ev} \times \Delta T_v \times (N-1)} \tag{41}$$

where A_{ev} is the surface area of each evaporator, ΔT_v is the mean vapor temperature difference of each evaporator (it is assumed that all the evaporators have the same), and the global heat transfer rate in the 13 evaporators is assessed as follows:

$$Q_{ev} = M_d \cdot \lambda_{ev} - Q_p - Q_c \tag{42}$$

where λ_{ev} is the latent heat at the average evaporator temperature and Q_c is the heat transfer rate in the condenser (equation (32)).

The overall heat transfer coefficient of the evaporators, U_{ev}, was correlated with an evaporator average vapor temperature $\bar{T}_v$ (mean between the vapor temperatures in the first and the last effect).

5. Results and Discussion

For the heater, the correlation which fitted the experimental data the best following El Nashar's variables dependency was:

$$U_h(M_f, M_h, T_{h,in}) = 176.03 - 4.33M_f - 30.84{M_f}^2 - 53.70M_h + 16.51M_fM_h + 2.89M_f^2M_h + 3.32M_h^2 - 1.43M_fM_h^2 + 0.16T_{h,in} - 0.06M_fT_{h,in} - 0.0004M_hT_{h,in} - 0.0001T_{h,in}^2 \quad (43)$$

In Fig 9 a comparison between the overall heat transfer coefficient measured for the heater and predicted by the correlation is shown. The adjustment fitted with an R-squared value of 0.74. As it can be seen, the correlation works fine for lower values of the heat transfer coefficient and slightly worse for larger values. It seems that different correlations should be taken into account to provide a better adjustment for the whole range of values.

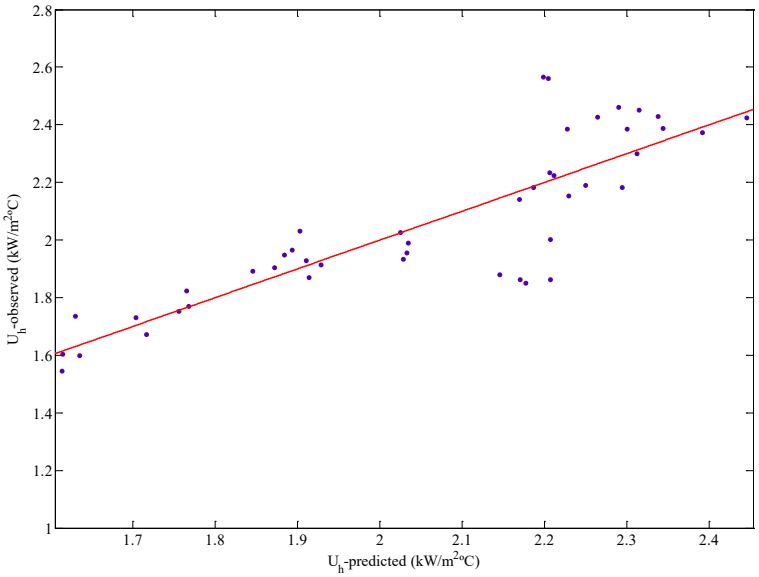

Fig 9: Comparison between the overall heat transfer coefficient of the heater observed and predicted by the correlation obtained in this work.

For the condenser, the following correlation based on El-Nashar's (i.e., sole dependence on the average temperature of the water in the condenser) was obtained:

$$U_c(T_{cw,in}, T_{cw,out}) = 0.81 + 0.02\left(\frac{T_{cw,in} + T_{cw,out}}{2}\right) \quad (44)$$

The correlation was not acceptable, however. A comparison between the observed and predicted overall heat transfer coefficient data showed a poor adjustment (R-squared of 0.22). As a result, other parameters were included in the correlation: the temperature of the vapor in the last effect (T_v *(N)*), and the cooling seawater flow rate (M_{cw}). The former is a better indicator of the temperature at which the condensation takes place. The latter is included because during the experiments it was not always constant. Since the experiments were performed in the summer, even though there was a dry cooler controlling the temperature build-up in the input flow of the condenser (as explained above), sometimes it was not possible to keep it constant. As a result, the cooling temperature was rising and in order to keep the temperature difference between the first and last cell constant during the operation, the cooling water flow rate to the condenser had to be adjusted.

A better correlation, fitting with an R-squared value of 0.70 (see Fig 10), was found considering these three variables:

$$U_c(T_{cw,in}, T_{cw,out}, M_{cw}, T_v(N)) = 0.93 - 0.0013 M_{cw} - 0.08\left(\frac{T_{cw,in} + T_{cw,out}}{2}\right) + 0.11 T_v(N) \tag{45}$$

However, the adjustment is still not very optimum and more experiments should be performed in order to determine the proper variables to be included in the correlation. In particular, more experiments should be carried out maintaining a constant cooling water flow rate, regardless the temperature difference between the first and last effect.

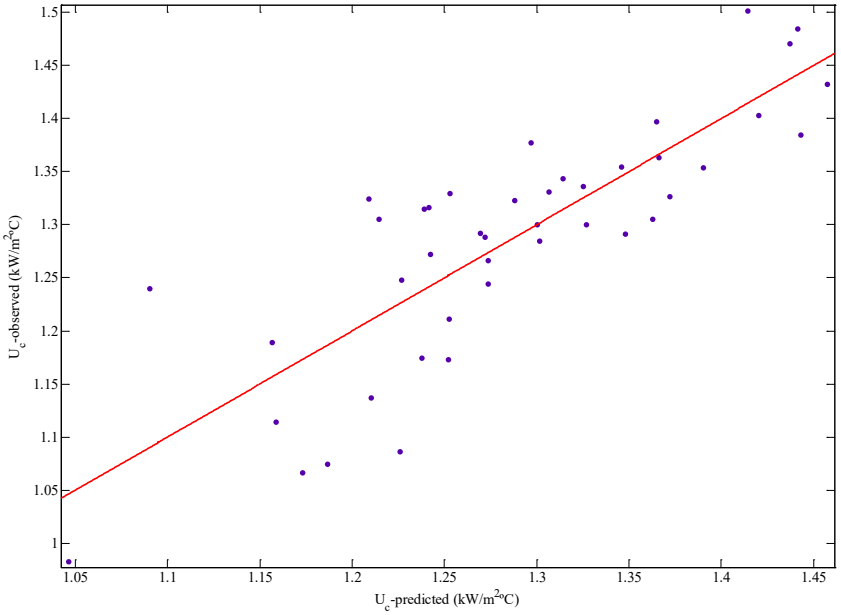

Fig 10: Comparison between the overall heat transfer coefficient of the condenser observed and predicted by the correlation

For the evaporators, the correlation between the average overall heat transfer coefficients was expressed by the equation:

$$U_{ev}(\overline{T}_v) = -55.36 + 3.63\overline{T}_v - 0.08\overline{T}_v^{\,2} + 5.48\cdot 10^{-4}\overline{T}_v^{\,3} \tag{46}$$

Fig 11 shows a comparison between the overall heat transfer coefficients observed and predicted by the correlation. The correlation proposed fitted quite well the experimental data obtained, with an R-squared of 0.83.

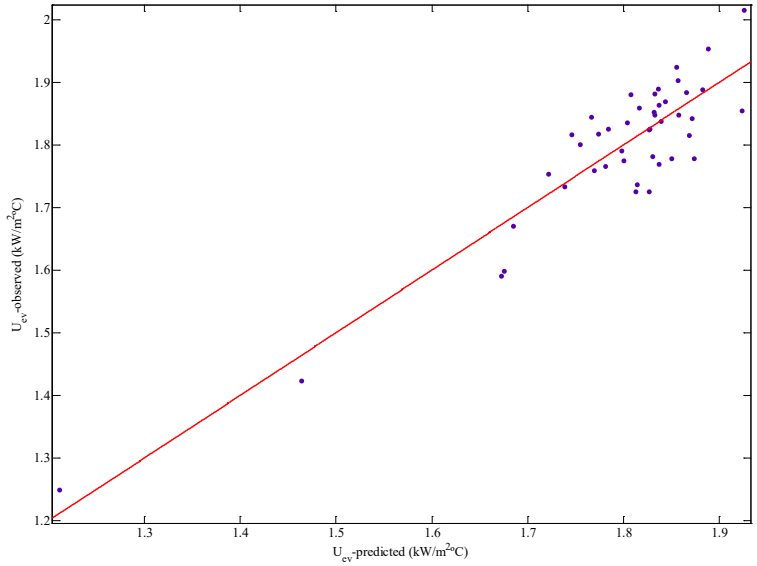

Fig 11: Comparison between the average overall heat transfer coefficient of the evaporators observed and predicted by the correlation

For the pre-heaters, the correlation to calculate the average overall heat transfer coefficient was given by:

$$U_p(M_f, \overline{T}_p) = 0.17 + 0.60M_f + 0.06{M_f}^2 + 0.002\overline{T}_p - 1.24{\cdot}10^{-5}\overline{T}_p^2 \quad (47)$$

A comparison between the overall heat transfer coefficients observed and predicted by the correlation is shown in Fig 12. The correlation proposed fitted very well the experimental data in the whole range, with an R-squared of 0.99.

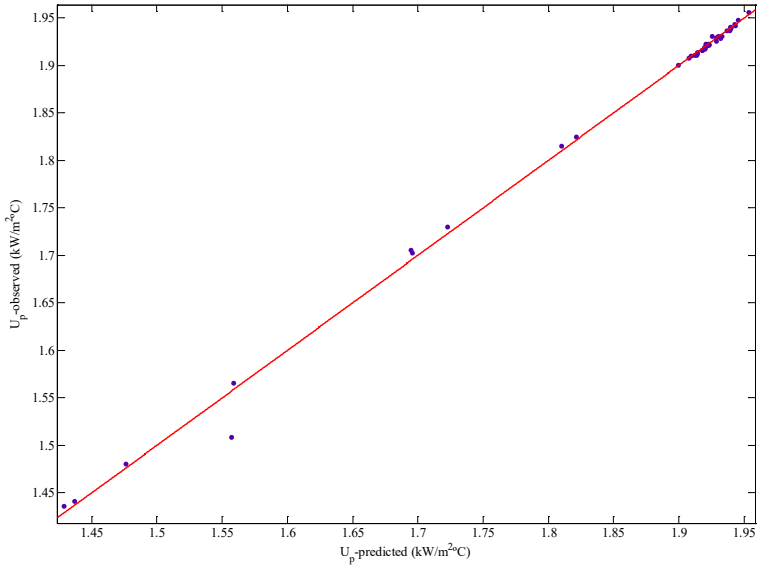

Fig 12: Comparison between the average overall heat transfer coefficient of the pre-heaters observed and predicted by the correlation

7. Conclusions

A mathematical model of the MED plant located at the PSA has been discussed. Correlations for the overall heat transfer coefficient of the different components were developed based on the characterization published by El-Nashar (2000). The correlations have been obtained from experiments carried out at the MED-PSA plant using a wide operational range (varying the heating water temperature from 57ºC to 74ºC, the heating water flow in a range of 7.8 L/s-12 L/s, the feed water flow in a range of 6 m^3/h-8 m^3/h, the cooling seawater flow rate from 10 m3/h to 25 m3/h and its temperature in a range of 12ºC-25ºC). The results showed a good agreement between the predicted and experimental data in the case of the evaporators and the pre-heaters.

In the case of the heater, the correlation obtained following El-Nashar's scheme showed to be not the most optimum for larger values of the overall heat transfer coefficients. In the case of the condenser, no adjustment was found using only the average temperature of water in the condenser, improving when the cooling water flow rate and the temperature of the vapor in the last effect were also considered. A thorough characterization with other relevant parameters should be performed in order to find better correlations for both the heater and the condenser.

Symbols Used

A	[m^2]	Heat transfer surface area
BPE	[ºC]	Boiling Point Elevation
h	[kJ/kg]	Enthalpy
m	[kg/s]	Mass flow rate
m'	[kg/s]	Mass flow rate in flashing processes
M	[kg/s]	Mass flow rate
N	[-]	Total number of effects
NEA	[ºC]	Non-equilibrium allowance
P	[bar]	Pressure
PR	[-]	Performance ratio
Q	[kW]	Heat transfer rate
T	[ºC]	Temperature
T'	[ºC]	Temperature in flashing processes
ΔT	[ºC]	Temperature difference
U	[kW/m^2ºC]	Overall heat transfer coefficient
X	[ppm]	Salt concentration

Greek Symbols

λ	[kJ/kg]	Latent heat of evaporation

Subscripts

b	Reject brine
'b	Vapor formed by flashing of the brine
br	Brine that has not flashed
c	Condensate or condenser
cw	Cooling seawater
d	Distillate
dcond	Distillate that leaves the 14^{th} effect
diny	Distillate that enters in 7^{th}, 10^{th} and 13^{th} effects
dmix	Distillate leaving the mixers
dph	Distillate produced in the pre-heater
ev	Vapor produced in the effect
f	Feed seawater
h	Heating water or heater
i	Effect

in	Inlet
out	Outlet
p	Pre-heater
v	Vapor leaving the pre-heater

References

[1] L. García-Rodríguez. Seawater desalination driven by renewable energies: a review. Desalination, 143 (2002) 103-113.

[2] J.W. Vermey. Taweelah-A1 makes breaksthrough in large-scale MED plants. Desalination & Water Reuse, 12 (2003) 10-13.

[3] G. Canton. Proceedings of IDA International Water Forum. Dubai, UAE, 2006,

[4] H. El-Dessouky, I. Alaitiqi, S. Bingulac and H. Ettouney. Steady-Stete Analysis of the Multiple Effect Evaporation Desalination Process. Quemical Engineering and Technology, 21 (1998) 437-451.

[5] A.M. El-Nashar and A.A. Qamhiyeh. Simulation of the steady-state operation of a multi-effect stack seawater distillation plant. Desalination, 101 (1995) 231-243.

[6] A.O.B. Amer. Development and optimization of ME-TVC desalination system. Desalination, 249 (2009) 1315-1331.

[7] E. Zarza, (Ed.), Solar Thermal Desalination Project, First Phase Results and Second Phase Description, 1st Ed. CIEMAT, Madrid, Spain, 1991.

[8] E. Zarza. Solar Thermal Desalination Project Phase II Results & Final Project Report. (1994)

[9] D. Alarcón-Padilla and L. García-Rodríguez. Application of absorption heat pumps to multi-effect distillation: a case study of solar desalination. Desalination, 212 (2007) 294-302.

[10] D.C. Alarcón-Padilla, L. García-Rodríguez and J. Blanco-Gálvez. Experimental assessment of connection of an absorption heat pump to a multi-effect distillation unit. Desalination, 250 (2010) 500-505.

[11] D. Alarcón-Padilla, L. García-Rodríguez and J. Blanco-Gálvez. Assessment of an absorption heat pump coupled to a multi-effect distillation unit within AQUASOL project. Desalination, 212 (2007) 303-310.

[12] D. Alarcón-Padilla, et al. First experimental results of a new hybrid solar/gas multi-effect distillation system: the AQUASOL project. Desalination, 220 (2008) 619-625.

[13] H. El-Dessouky and H. Ettouney. Fundamentals of Salt Water Desalination, ELSEVIER SCIENCE B.V, Amsterdam, The Netherlands, 2002.